Crown ether–electrolyte interactions permit nanopore detection of individual DNA abasic sites in single molecules

Na An, Aaron M. Fleming, Henry S. White[1], and Cynthia J. Burrows[1]

Department of Chemistry, University of Utah, Salt Lake City, UT 84112-0850

Edited by Royce W. Murray, The University of North Carolina at Chapel Hill, Chapel Hill, NC, and approved May 29, 2012 (received for review February 26, 2012)

DNA abasic (AP) sites are one of the most frequent lesions in the genome and have a high mutagenic potential if unrepaired. After selective attachment of 2-aminomethyl-18-crown-6 (18c6), individual AP lesions are detected during electrophoretic translocation through the bacterial protein ion channel α-hemolysin (α-HL) embedded in a lipid bilayer. Interactions between 18c6 and Na^+ produce characteristic pulse-like current amplitude signatures that allow the identification of individual AP sites in single molecules of homopolymeric or heteropolymeric DNA sequences. The bulky 18c6-cation complexes also dramatically slow the DNA motion to more easily recordable levels. Further, the behaviors of the AP-18c6 adduct are different with respect to the directionalities of DNA entering the protein channel, and they can be precisely manipulated by altering the cation (Li^+, Na^+ or K^+) of the electrolyte. This method permits detection of multiple AP lesions per strand, which is unprecedented in other work. Additionally, insights into the thermodynamics and kinetics of 18c6-cation interactions at a single-molecule level are provided by the nanopore measurement.

alpha-hemolysin | crown ethers | single-molecule detection | DNA damage

As one of the most frequent lesions in the genome, DNA abasic (AP) sites are derived from either spontaneous hydrolysis of the glycosidic bonds, often as a result of alkylation or oxidation of purines, or the enzymatic removal of modified bases by glycosylase enzymes in the base excision repair (BER) pathway (1–3). Failure to repair AP sites poses a severe challenge to polymerases and also leads to strand breaks, DNA cross-links, and transcriptional mutations, resulting in cellular dysfunction (1, 2, 4). Common detection methods for AP sites include using aldehyde-reactive probes (5, 6) followed by an ELISA-like assay (7), fluorescence microscopy (8), or atomic force microscopy (9); various metalloinsertors (10), mass spectrometry (11), and isotope labels (12) can also help visualize this lesion. There is urgent need for methods that provide surrounding sequence information and have the ability to detect multiple damage sites per strand, a phenomenon of significant biological importance (13). Furthermore, given their abundance in human cells (~18,000 per cell per day) and ability to stall polymerases, AP lesions become a technical hurdle to DNA sequencing efforts that require PCR amplification and sequencing-by-synthesis processes.

Emerging as a rapid and inexpensive single-molecule DNA analysis platform, nanopore ion channel technology has been under intensive investigation with the biological pore α-hemolysin (α-HL), which proceeds by electrically drawing an individual single-stranded DNA (ssDNA) strand through this self-assembled bacterial protein ion channel embedded in a lipid bilayer (14, 15). Due to the limited size of the constriction of α-HL (~1.4 nm) (16), the translocation of ssDNA through the channel significantly reduces the electrolyte ion flow, resulting in a deep current blockage, potentially revealing the identity of the nucleotide sequence (17–19). Recently, this method has also been explored to examine epigenetic markers (20), DNA oxidative damage products (21, 22), secondary structures (23), enzymatic activity (24–26), and chemical reactions (27).

Chief advantages of the α-HL protein nanopore include its excellent stability, reproducibility, and precise tuning properties via site-directed mutagenesis, in addition to the minimal requirements of expensive reagents and data storage and handling equipment. The high speed (1–20 μs/nucleotide) at which ssDNA is driven through the ion channel above the threading voltage promises rapid and long reads; however, it is this very feature of free translocation that prohibits resolution of single bases that exhibit characteristic signatures of less than a few picoamperes current difference using available electronics (14). Most efforts to approach these challenges are devoted to engineering the protein (28–30), embedding adapters (31), synthesizing peptide-conjugated nucleotides (32), controlling DNA movement with molecular motors (33, 34), and exploring experimental conditions (35, 36). Among these studies, the stable AP analog tetrahydrofuran (THF) has been used as a marker to inspect DNA polymerase activities and to map the recognition sites of the α-HL ion channel (24–26); the native AP lesion has never been studied in α-HL or related ion channels.

Due to the prevalent role of AP sites in normal and disease-related processes, the ability to obtain sequence information surrounding this lesion at a single-molecule level would be of great importance in understanding disease mechanisms and in medical diagnostics, for which no convenient method currently exists. The α-HL nanopore presents a potential solution to this challenge. In previous work, we showed that adducts to 8-oxo-7,8-dihydro-2′-deoxyguanosine (OG) produced different current levels than native bases while being immobilized inside of the α-HL ion channel. However, all of these OG adducts failed to generate resolvable current signatures during free translocations (21). In this work, we demonstrate that the selective attachment of an 18-crown-6 (18c6) moiety to an AP site produces very unique current amplitude signatures that allow the identification of individual sites along a single homopolymeric or heteropolymeric DNA strand as a result of the specific interactions between the crown ether and electrolyte cations. This is the first demonstration of current modulation during ssDNA translocation via adduct formation to native strands. Furthermore, the AP-18c6 adduct translocation behavior can be precisely manipulated by simply altering the electrolyte cation. Additionally, the speed of DNA translocation was dramatically slowed as the AP-18c6 adduct

Author contributions: N.A., A.M.F., H.S.W., and C.J.B. designed research; N.A. and A.M.F. performed research; N.A. analyzed data; and N.A., A.M.F., H.S.W., and C.J.B. wrote the paper.

The authors declare no conflict of interest.

This article is a PNAS Direct Submission.

[1]To whom correspondence may be addressed. E-mail: burrows@chem.utah.edu or white@chem.utah.edu.

This article contains supporting information online at www.pnas.org/lookup/suppl/doi:10.1073/pnas.1201669109/-/DCSupplemental.

www.pnas.org/cgi/doi/10.1073/pnas.1201669109

passes through the protein nanopore, resulting in millisecond-long current signatures that are readily observed.

Results and Discussion

Modification of AP Sites with a Crown Ether Adduct. It is thought that 10–15 nucleotides contribute to the current blockage signal when ssDNA translocates through the α-HL ion channel (28); thus, a single AP lesion is unlikely to be resolved from the native nucleotides via a modest change in the current amplitude. The goals of chemical modification of DNA bases are both to amplify the signal differences and to stabilize the AP site against strand breaks. AP sites tautomerize between the ring-closed hemi-acetal form and the ring-opened aldehyde form; the latter offers the possibility of functionalization via reductive amination coupling with 2-aminomethyl-18-crown-6 to form the stable adduct AP-18c6 (Fig. 1). In the present work, uridine-containing oligodeoxynucleotides (ODNs) were treated with uracil-DNA glycosylase (UDG) to generate AP sites. With the possible exception of trace amounts of 5-formyl-pyrimidines, oxidation products of 5-methylC, and thymidine (37), the AP site presents the only aldehyde group existing in DNA, and reductive amination occurs in very high yield and specifically at the AP site using $NaBH_3CN$ in the presence of a primary amine. We chose 2-aminomethyl-18c6 as the amine of choice due to its water solubility and ability to interconvert between a large, rigid, disc-like structure when bound to alkali metal ions and a flexible, collapsed one when the metal ion dissociates.

Ion Channel Recording of Immobilized AP and AP-18c6. As a preliminary study, the electrical current signatures of the AP site and AP-18c6 were measured in a static experiment in which ssDNA was immobilized inside the protein nanopore using streptavidin-biotin (Strep-Btn) complex formation, suspending ssDNA in the ion channel to accurately measure the current blockage level (28, 38, 39). A voltage (120 mV *trans* vs *cis*) applied across a lipid bilayer spanning the orifice of a glass nanopore membrane (GNM) drove the ssDNA to enter the *cis* side of the protein nanopore, reducing the open channel current I_o to a lower level I. Both I and I_o were recorded, and $\%I/I_o$ is quoted as the percentage residual current (Fig. 2). The Strep-Btn ssDNA complex was retained for ~1 s; the polarities of the electrodes were then reversed for ~150 ms to remove DNA from the channel, and the voltage polarity was switched back again for the next event.

The 5 nm long β barrel of wild-type α-HL possesses multiple recognition sites that simultaneously contribute to the residual current, and one of the most current-sensitive regions resides at position 14 of the DNA strand relative to the biotin linkage (28). Consequently, AP and AP-18c6 were placed at this position in the immobilization analysis. More than 200 capture/release events were collected for each sample, and the 5′- or 3′-biotinylated poly-C_{40} (5′- or 3′-Btn-C_{40}), whose $\%I/I_o$ values were set to 0, were used as the internal standards for the corresponding substituted strands.

A single AP lesion was generated by treating 3′-Btn $C_{39}U_{\omega 14}$ with UDG, and current measurements for $\Delta\%I/I_o$ were performed immediately afterwards. The AP site without an adduct showed an average current level in 1 M KCl that was 1.1% less blocking than the control 3′-Btn-C_{40} (Fig. S1*A*). Previous efforts

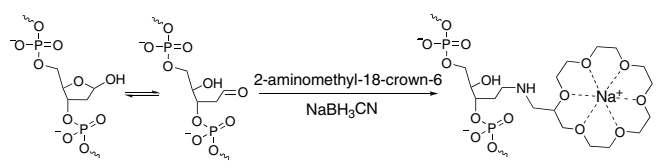

Fig. 1. Synthetic scheme for AP-18c6 adduct.

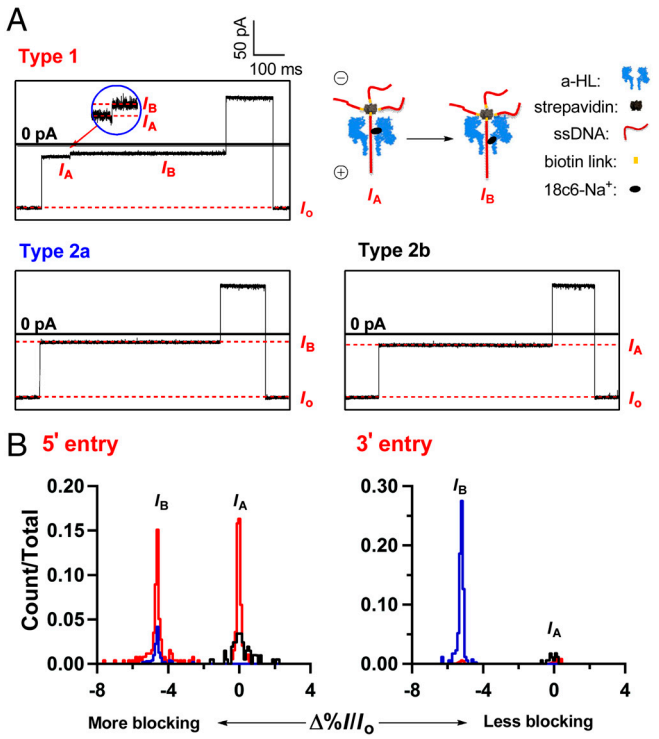

Fig. 2. Immobilization studies of AP-18c6 with 1 M NaCl as electrolyte. (*A*) Three types of *i*-*t* traces presented by AP-18c6. (*B*) Histograms of current blockage levels of both 3′ and 5′ entries. Color code: red (type 1), blue (type 2a), and black (type 2b).

suggested that the $\Delta\%I/I_o$ of DNA native bases fall into the range of 0–1.2% $\Delta\%I/I_o$ relative to C (21, 28), and thus unfortunately, the AP site yielded a current blockage almost identical to G under these circumstances. This suggests that an AP site would produce a false readout as G in sequencing efforts with wild-type α-HL, and given the multiple sources and abundance of AP sites in cells, this would be problematic.

The behaviors of ssDNA strands are rather different with respect to directionality when entering the protein channel, in terms of both event frequency and current blockage (38, 40). Thus, the current signatures of both 5′-Btn-C_{39}AP-18c6$_{14}$ (3′ entry) and 3′-Btn-C_{39}AP-18c6$_{\omega 14}$ (5′ entry) were recorded with 5′- and 3′-Btn-C_{40} as the references, respectively, in 1 M NaCl. Unlike the immobilization events of unmodified ssDNA and other adducts we have previously studied, AP-18c6 presented two different types of individual *i*-*t* traces (Fig. 2*A*). Type 2 events exhibited a constant current level of magnitude I_A or I_B that indicated the capture of ssDNA. More interestingly, a transition between two current blockage levels ($I_A \rightarrow I_B$) was observed in type 1 events. Given that I_A had the same residual current as the control poly-dC_{40} ($\Delta\%I_A/I_o = 0$), this result suggests that the initial current level I_A in type 1 events corresponds to the 18c6-Na^+ complex hesitating above the constriction of α-HL, while the sensing β barrel was recording signals of the poly-dC part of the strand. The 18c6-Na^+ complex can convert between several conformations of similar shape, one of which ($1C_1$) features a tight coordination associated with a significantly shorter O-Na^+ distance than the quasiplanar symmetric D_{3d} conformer that 18c6-K^+ almost exclusively adopts. In the Na^+ complex, 18c6 is curved to provide a balance between the O-Na^+ attraction and O–O repulsion, resulting in a more compact shape. The other conformer is D_{3d} with a lower stability constant (K_s) due to the longer distance between oxygen atoms and Na^+ compared to 18c6-K^+ (41). We therefore hypothesize that after entering the vestibule, a period of time is required for 18c6-Na^+ to optimize

its conformation, allowing it to enter into the narrow β barrel and position itself at the recognition site, causing a much deeper current blockage level (I_B, $\Delta\%I_B/I_o \sim -4.6\%$) that lasts for the remainder of the event before voltage reversal (type 1). As demonstrated below, the $I_A \rightarrow I_B$ transition provides a signature for detecting 18c6 adducts during translocation of DNA. Type 2a events correspond to entry of 18c6-Na^+ into the vestibule of α-HL with an orientation that allowed it to pass into the constriction without hesitation, resulting immediately in current level I_B. Contrarily, type 2b events correspond to the adducted complex located at a position such that interactions between the protein, 18c6 and Na^+ prevented it from entering into the β barrel before the reversal of polarity; the poly-dC portion of the DNA strand was solely contributing to the signal resulting in current level I_A.

Similarly to unmodified ssDNA, the directionality of AP-18c6 entering into the protein channel also affects its current signature (Fig. 2*B*) with 3′ entry displaying a smaller residual I_B ($\Delta\%I_B/I_o \sim -5.3\%$). Many more 5′ entry events (58%) presented the desirable two-step current feature (type 1) compared to those of 3′ entry (<2%). In nearly 90% of 3′ entry events, the 18c6-Na^+ complex appears to pass immediately through the constriction into the β barrel (type 2a), while only 12% of 5′ entry events were able to do so. Also, there were many AP-18c6 events (30%) that could not enter the β barrel from the 5′ end (type 2b); yet, only ~8% of the events had the same problem from the other terminus. These directionality effects can be explained by the tendency of ssDNA bases to tilt towards the 5′ end in a strongly confined environment, producing the "Christmas tree" geometry (40). As a result, DNA strands entering from the 5′ direction experience more friction from the protein, along with steric hindrance from the bulky 18c6-Na^+, causing more type 2b events to occur than during 3′ entry. The direction of DNA entry may position the crown ether differently relative to the protein constriction, and slight differences in the position/orientation of 18c6 would likely change its interaction with the protein, thus affecting the current signature during translocation.

Immobilized DNA measurements were also performed in 1 M KCl and LiCl to interrogate the interactions between 18c6 and cations as an approach to altering the electrical signature of AP-18c6, and also to provide insight into the correlation between these interactions and the electrical signals. Because 5′ entry produced a more sensitive and desirable signature as described above, the current blockages of 3′-Btn C_{39}AP-18c6$_{\omega 14}$ were recorded in 1 M KCl and LiCl, respectively, and not surprisingly, the two 18c6-M^+ experiments showed very distinct $\Delta\%I/I_o$ histograms compared to 18c6-Na^+ (Fig. S2). While 18c6-Li^+ presented a single $\Delta\%I/I_o$ peak, 2.1% more blocking than the control, 18c6-K^+ had one broader distribution of $\Delta\%I/I_o$, centered at −4.1%, and one peak lining up with the 3′-Btn-dC_{40} control. These observations can be explained as follows. Due to its small size and high desolvation energy, Li^+ does not form a very stable complex with 18c6 (42). Thus, the slightly deeper current blockage of the AP-18c6 adduct observed in LiCl electrolyte compared to unmodified DNA is likely due to the added steric bulk of the uncomplexed crown ether in an elliptical conformation. No two-step current signature is observed in LiCl, suggesting that there is little or no barrier for the free crown ether to enter the β barrel of α-HL. In the case of K^+, the 18c6-K^+ complex exists as a single quasiplanar symmetric D_{3d} conformer, resulting from the ideal size matching between the cation and the polyether cavity. Additionally, this conformer provides ideal solvation, and consequently, stabilizes the system and maximizes its size (~5.3 Å in radius) (41). Given the high K^+ concentration and the high-energy cost for 18c6-K^+ to change conformation (>13 kJ mol^{-1}), we anticipated that the passage of the 18c6-K^+ through the constriction of the α-HL would be difficult. In Fig. S2*B*, only the poly-dC tail is responsible for the small current blockage peak at $\Delta\%I/I_o = 0$, equivalent to an unmodified 3′-Btn-C_{40} strand with the 18c6-K^+ complex sitting above the constriction. The broader peak of the histogram, which contains the majority of the events, suggests that when the metal complex is forced into the constriction zone, it is not in a reproducible orientation that gives a single deep current blockage. Together, these results demonstrate that the interactions between 18c6 and electrolyte cations can be correlated to their electrical signatures, and that the unique two-level current feature of 18c6-Na^+ can be used to detect AP sites at a single-molecule level.

Translocation Studies of AP-18c6 in a Homopolymeric Strand. Immobilization studies allowed us to examine closely the potential of detecting AP lesions using the characteristic current signature obtained by the interaction between 18c6 and various alkali metal cations. In the series, Li^+ is too weakly complexed by 18c6 to affect the current signature, K^+ is too strongly bound by 18c6 leading to a rigid complex that is too large to reproducibly enter the constriction of the ion channel, and Na^+ is "just right," demonstrating both a step change in current blockage level and a readily measurable delay time for proper entry into the β barrel. Next, we examined the behavior of ssDNA while translocating through the α-HL ion channel. To be consistent with the immobilization studies, individual AP-18c6 were also embedded in a poly-dC context, and two DNA constructs were studied: a mono adduct 5′-d($C_{43}XC_{43}$) and a bis adduct 5′-d($C_{25}XC_{35}XC_{25}$), where X = AP-18c6. Measurements were performed in a buffer containing 3 M NaCl as the electrolyte over a range of applied voltages (80, 100, 120, 160 mV *trans* vs. *cis*).

The translocation of unmodified homopolymeric strand dC_{87} was investigated first as a control, focusing on current level (I), duration time (t_D) and directionality effects. Individual *i-t* traces from either 3′ or 5′ entry displayed a single constant current during translocation with $t_D \sim 0.25$ ms, consistent with a translocation velocity of ~4 μs/nucleotide (Fig. 3*A*). Two populations of events were observed in the I vs. t_D density plots, (Fig. 3*B*); in accordance with the immobilization studies of 5′-Btn-C_{40} and 3′-Btn-C_{40} under the same conditions ($\%I/I_o = 15.6$ and 16.2, respectively), 3′ entry of this homopolymer produced a deeper current blockage (Fig. S1*B*). Thus, these clusters were assigned to represent 3′ and 5′ entry of the strand into the protein vestibule, respectively. Consistent with diffusional broadening of translocation times, the t_D histogram of each population was well described by a Gaussian curve with the peak value t_{max}, which decreased with increased applied voltages for both directions (Fig. 3*C*). Entry from the 3′ terminus was favored under lower

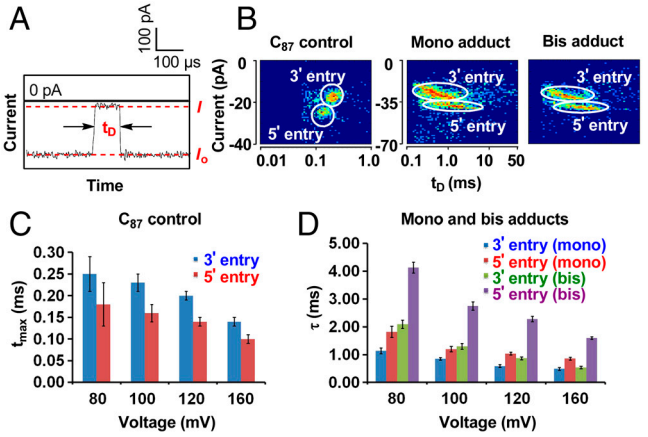

Fig. 3. Translocation studies of AP-18c6 in homopolymeric strands with 3 M NaCl as the electrolyte. (*A*) Typical *i-t* trace of the control strand and definition of translocation duration (t_D). (*B*) Sample density plots of control and adducted strands (120 mV *trans* vs. *cis*). (*C*) Plot of t_{max} vs. voltage for the control strand. (*D*) Plot of τ vs. voltage for the mono and bis adducts.

driving force, resulting in higher event frequencies, while the slightly faster 5′ population grew with increasing voltage until such discrimination faded around 160 mV (*trans* vs. *cis*) (Figs. S3–S6).

Similarly, both mono and bis-adduct strands also showed distinct directionality effects with 3′ entry events occurring more frequently under low voltages and generating deeper current blockages (Fig. 3*B*). However, the population clusters of both directions presented more oval-shaped distributions that were better approximated by a single exponential decay with a time constant $\tau_{5'}$ or $\tau_{3'}$ (5′ or 3′ entry, respectively) of several milliseconds, indicating that the slow conformational motion of AP-18c6 required for it to pass through the constriction region of α-HL determines the overall translocation time. In contrast to the values for the C_{87} control, $\tau_{5'}$ was considerably longer than $\tau_{3'}$ for both mono and bis-adducted strands (Fig. 3*D*).

Individual *i-t* traces of both mono and bis-adduct strands exhibited rather different features depending on the entry direction (Fig. 4). For 3′ entry, the presence of the AP-18c6 adduct was not evident in the shape of the *i-t* trace (Fig. 4*A*). However, *i-t* traces with unique pulse-shaped signatures were observed upon translocation of AP-18c6 from the 5′ terminus (Fig. 4*B*). Taking the *i-t* trace of the mono adduct at 120 mV as an example, an initial current blockage level of I_{A1} was observed with characteristic exponential time distribution (~2.5 ms, Table S1). Given that the value of $\%I_{A1}/I_o$ was consistent with the percentage residual current of the immobilized 3′-Btn-C_{40} ($\%I/I_o = 16.2\%$), this segment of the *i-t* trace is assigned to be the temporary pausing of poly-dC in the narrow constriction zone of the ion channel, while 18c6-Na^+ remains in the larger vestibule, waiting to undergo ion dissociation and/or conformational change that would permit entry into the narrower, sensing part of the channel. The mid-section of the event (I_{B1}) showed a nearly 9% deeper current blockage, and exponential decay constant of ~0.59 ms, which we interpret to be associated with the bulky crown ether moving through the narrow β barrel. Notably, the percentage residual current changes ($\%I_A/I_o$-$\%I_B/I_o$) in the presence of 18c6 adduct during translocation fell into the same range compared to the immobilization experiment (~4.6%), which statically positioned the adduct at a single location. Finally, when the AP-18c6 exited the constriction zone, the current level returned to that of poly-dC (I_{A2}) for a short period of time while the C_{43} tail completed translocation, resulting in an overall $I_{A1} \rightarrow I_{B1} \rightarrow I_{A2}$ pulse shape. The short I_{A2} segment was well described by a Gaussian distribution of times, with $t_{max} \sim 0.06$ ms, consistent with a free translocation velocity of ~1.5 μs/nucleotide. For the bis adduct, the 35 cytosines between two AP-18c6 adducts were sufficient to position the first adduct out of the *trans* side of α-HL, while the second trailing adduct undergoes conformational changes and passes through the constriction, causing a second current modulation ($I_{A2} \rightarrow I_{B2} \rightarrow I_{A3}$). Overall the bis adduct displays two pulse-shaped modulations ($I_{A1} \rightarrow I_{B2} \rightarrow I_{A2} \rightarrow I_{B2} \rightarrow I_{A3}$), corresponding to the sequential translocation of the two AP-18c6 adducts (Fig. 4*B*).

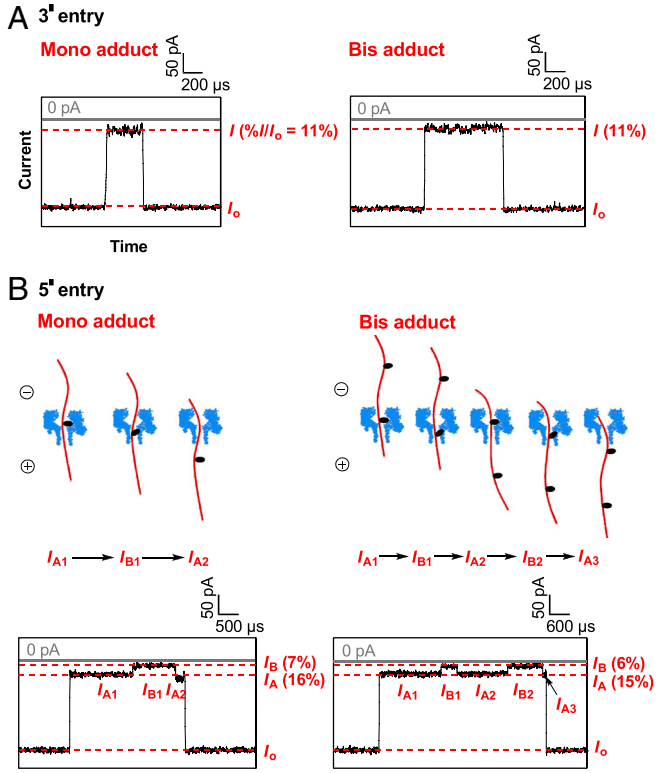

Fig. 4. Individual *i-t* traces of AP-18c6 in homopolymeric strands. (*A*) Sample *i-t* traces of 3′ entry for mono and bis adducts (120 mV *trans* vs. *cis*). (*B*) Sample *i-t* traces of 5′ entry for mono and bis adducts (120 mV *trans* vs. *cis*).

Consistent with the immobilization studies, not every 5′ entry event of AP-18c6 adduct has to hesitate for a long time to pass the constriction if 18c6-Na^+ enters into the vestibule with the proper orientation and conformation. Accordingly, 20% of the mono-adduct events did not have a resolvable pulse-like modulation in the current, nor did 5% of the bis-adduct events. Additionally, ~26% of the bis-adduct events showed only one current modulation, similar to the mono-adduct, but with slightly longer duration, indicating one of the adducts had the proper orientation and conformation to pass unimpeded through the constriction. Translocation studies were performed at different voltages (80, 100, 120, 160 mV *trans* vs. *cis*) in order to verify that the adducted strands did successfully reach the *trans* side of α-HL instead of being held in the vestibule and diffusing back to the *cis* side. We observed that the duration of both directions was inversely correlated with the driving force (Fig. 3*D*), suggesting full translocations of the 18c6-Na^+ adducted DNA.

In the above analyses, the duration of the current segments I_{A1} (for the mono adduct) and I_{A1} and I_{A2} (for the bis adducts) are associated with 18c6-Na^+ conformational changes, including the likely dissociation of the complex, prior to 18c6 moving through the constriction of α-HL. At 120 mV, these times are 2.50 ms (I_{A1}) for the mono adduct, and 2.75 (I_{A1}) and 1.78 ms (I_{A2}) for the bis adduct (Table S1), much longer than the value expected (2.9×10^{-8} s) based on the Na^+ dissociation rate constant in bulk solution (43). This 5 order of magnitude difference indicates that the constricted geometry of the ion channel dramatically decreases the dissociation of the 18c6-Na^+ complex.

Translocation Studies of AP-18c6 in a Heteropolymeric Strand. Both immobilization and translocation studies showed promising results for using the interactions between 18c6 and electrolyte cations to detect individual AP sites in a homopolymeric oligo-dC strand. Next, we further explored the sequence context effect on the adduct behavior by embedding one AP-18c6 adduct in a heteropolymeric DNA strand that was designed to be free of secondary structure for simplicity (Fig. 5*A*). Similarly to the homopolymeric context, both adducted and unmodified strands showed a distinct directionality effect with respect to current blockages, and translocation times that decreased at higher voltages (Fig. 5 *B* and *D*). The more dynamic and flexible secondary structures of the heterosequence, compared to the stick-like structure proposed for a poly-dC strand (44), results in an intermediate current level I_M before the deep blockage in the individual *i-t* traces. As previously reported, the intermediate level I_M corresponds to the presence of DNA in the large vestibule, exploring orientations to thread into the β barrel (Fig. 5*C*) (23). Most significantly, the 5′ entry events still exhibited the pulse-

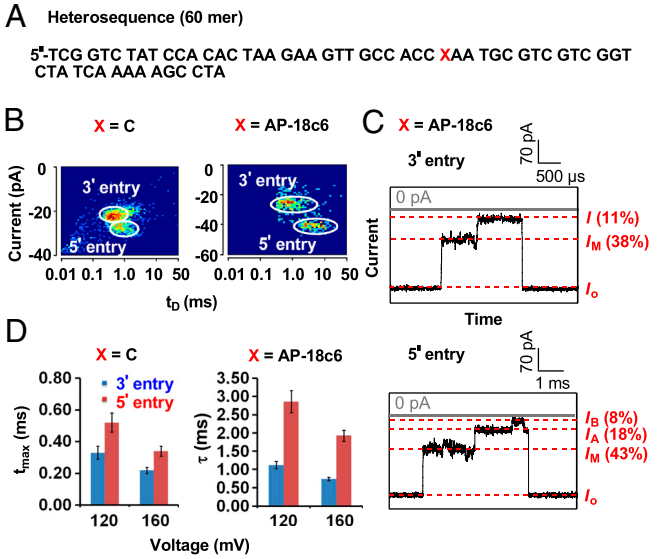

Fig. 5. Translocation studies of AP-18c6 in heteropolymeric sequence with 3 M NaCl as electrolyte. (*A*) Heteropolymeric sequence (60 mer). (*B*) Sample density plots of control (X = C) and adducted strand (X = AP-18c6) (120 mV *trans* vs. *cis*). (*C*) Individual *i-t* traces of the adducted strand. Top: 3′ entry event. Bottom: 5′ entry event. (*D*, *Left*) Plot of t_{max} vs. voltage for the control strand. (*Right*) Plot of τ vs. voltage for adducted strand.

shaped current modulation ($I_{A1} \rightarrow I_B \rightarrow I_{A2}$) due to the presence of the AP-18c6 adduct. These results are important as a demonstration that the current amplitude signature of AP-18c6 is due to its unique motif and interactions with the electrolyte cations; thus, it can potentially serve as a universal tool for AP site identification, independent of sequence context.

Manipulation of AP-18c6 Behaviors By Altering the Electrolyte. The distinct behaviors of AP-18c6 with different electrolytes in the immobilization studies provided us with insight into the correlation between 18c6-M^+ interaction and its electrical signal, and these specific properties also presented the possibility to tune the current signature of the adduct by altering the electrolyte contents. In addition to NaCl, translocation studies of the mono adduct (5′ $C_{43}XC_{43}$, X = AP – 18c6) were also performed in KCl and LiCl, and consistent with the immobilization results, 18c6-K^+ was not able to reproducibly enter the constriction zone due to its stable D_{3d} conformation and the high [K^+]. At higher voltages, the 18c6-K^+ could be held in the vestibule and released only upon the reversal of the polarities, causing 'immobilization-like' *i-t* traces (Fig. S7*A*). On the other hand, 18c6-Li^+ showed no barrier in translocating through the channel, leaving unidentifiable current signatures (Fig. S7*B*).

Next, the same experiments were performed in LiCl electrolytes doped with varying amounts of KCl. Given the selectively strong interaction between 18c6 and K^+ and the much weaker binding affinity of 18c6 towards Li^+, the latter could be neglected; thus, the fractional percentage of K^+-bound 18c6 could be calculated based on the equilibrium stability constant (K_s = 114.8 M^{-1}) under these conditions (Fig. 6*B*) (43). With a low driving force (80 mV *trans* vs. *cis*), three distinct populations of events (A, B and C) appeared with different durations (Fig. 6*A*), and the ratio of event counts changed with the electrolyte content. While populations A and B showed normal translocation *i-t* traces, C presented "immobilization-like" ones. Based on the results obtained in the pure LiCl electrolyte, population A is assigned to the K^+-free AP-18c6. Populations B and C were much longer, and their combined percentage event counts, for the fractional percentage of K^+ ranging from 0.1 to 20%, were in excellent agreement with the percentage of K^+-bound 18c6

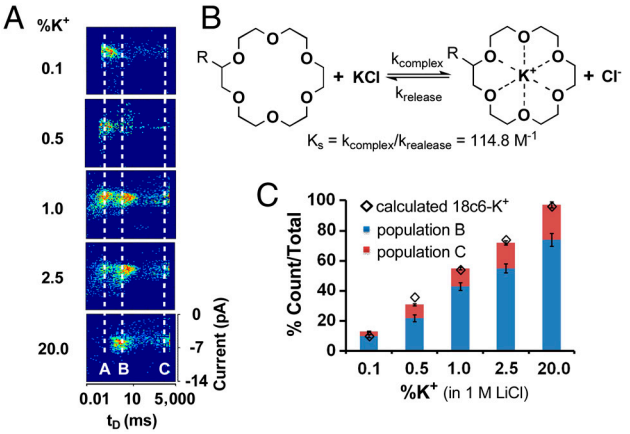

Fig. 6. Electrolyte-dependent translocation studies of the mono adduct strand. (*A*) Density plots of various %K^+ (in 1 M LiCl) conditions under 80 mV (*trans* vs. *cis*). (*B*) Complexation and dissociation of 18c6-Na^+ (R = DNA) with the equilibrium constant K_s (43). (*C*) Plot of combined percentage event counts of populations B and C vs. %K^+ (in 1 M LiCl), compared to calculated values.

calculated based on K_s (Fig. 6*C*), suggesting they were both due to 18c6-K^+ complexes. Because the ratios of population C to B were always roughly 3:1 under these conditions, we suggest that they correspond to the directionality effect with B being 3′ and C being 5′ entry of the DNA strand into the vestibule. The agreement between nanopore-measured and K_s-based calculated values of the percentage of K^+-bound 18c6, coupled with the above-noted orders of magnitude slower dissociation time of the Na^+-complex in the nanopore relative to bulk solution, indicate that the measured values of the percentages of K^+-bound 18c6 are determined by equilibrium concentrations of bound and unbound 18c6 external to the α-HL ion channel.

In summary, these results demonstrate a crucial role for 18c6-M^+ interactions in producing electrical signatures of 18c6-adducted DNA while translocating through a protein nanopore, and also provide a promising tool to manipulate the behavior of the adduct precisely on a single-molecule level. By attaching 18c6 to an AP site, the electrical signature of ssDNA translocation could be dramatically modified. Specifically, pulse-like current modulations during translocation of DNA caused by the presence of individual AP-18c6 adducts demonstrate the possible application of this method as a detection tool for multiple AP sites on single molecules of DNA. Employing the same chemical strategy combined with the assistance of lesion-specific glycosylases, one can envision that a variety of DNA base damages and mismatches can be specifically converted to AP sites and then functionalized to the AP-18c6 adduct, permitting their sequence-specific detection in single molecules.

Materials and Methods

Full experimental procedures of AP adduct preparation and characterization, ion channel recordings, and sources of materials can be found in the *SI Text*.

Ion Channel Recordings. A custom-built, high-impedance, low-noise amplifier and data acquisition system, designed and constructed by Electronic Biosciences (EBS), San Diego, CA, was used for the current–time (*i-t*) recordings. In the immobilization studies, Strep-Btn DNA (40 pmol, 200 nM) was added in the cell and more than 200 capture/release events were collected under 120 mV bias (*trans* versus *cis*) with a 10 kHz low pass filter, and 50 kHz data acquisition rate. Then, the same amount of Strep-Btn dC_{40} control was added as an internal standard. For the translocation studies, ssDNA (2 nmol, 10 μM) was added and more than 1,000 events were collected for each voltage with a 100 kHz low pass filter, and 500 kHz data acquisition rate.

Data analysis. Density plots were analyzed with software donated by EBS. Events were extracted using QUB 1.5.0.31 and fitted using Igor Pro 6.1. Individual translocation *i-t* traces were refiltered to 50 kHz for presentation.

ACKNOWLEDGMENTS. The authors gratefully acknowledge the technical discussions with Dr. Geoffrey Barrall and colleagues at EBS and the donation of instruments and software by EBS, San Diego, CA. This work was supported by NIH (GM093099 and HG005095).

1. Boiteux S, Guillet M (2004) Abasic sites in DNA: Repair and biological consequences in *Saccharomyces cerevisiae*. *DNA Repair* 3:1–12.
2. Wilson DM, III, Barsky D (2001) The major human abasic endonuclease: Formation, consequences and repair of abasic lesions in DNA. *Mutat Res* 485:283–307.
3. Clauson CL, Oestreich KJ, Austin JW, Doetsch PW (2010) Abasic sites and strand breaks in DNA cause transcriptional mutagenesis in *Escherichia coli*. *Proc Natl Acad Sci USA* 107:3657–3662.
4. Gates KS (2009) An overview of chemical processes that damage cellular DNA: Spontaneous hydrolysis, alkylation, and reactions with radicals. *Chem Res Toxicol* 22:1747–1760.
5. Kubo K, Ide H, Wallace SS, Kow YW (1992) A novel, sensitive, and specific assay for abasic sites, the most commonly produced DNA lesion. *Biochemistry* 31:3703–3708.
6. Komatsu Y, Ohtsuka E, Mikami A, Takebayashi T, Kojima N (2009) Construction of highly reactive probes for abasic site detection by introduction of an aromatic and a guanidine residue into an aminooxy group. *J Am Chem Soc* 131:13208–13209.
7. Atamna H, Cheung I, Ames BN (2000) A method for detecting abasic sites in living cells: Age-dependent changes in base excision repair. *Proc Natl Acad Sci USA* 97:686–691.
8. Greco NJ, Tor Y (2005) Simple fluorescent pyrimidine analogues detect the presence of DNA abasic sites. *J Am Chem Soc* 127:10784–10785.
9. Sun HB, Qian L, Yokota H (2001) Detection of abasic sites on individual DNA molecules using atomic force microscopy. *Anal Chem* 73:2229–2232.
10. Zeglis BM, Boland JA, Barton JK (2008) Targeting abasic sites and single base bulges in DNA with metalloinsertors. *J Am Chem Soc* 130:7530–7531.
11. Bowler FR, Diaz-Mochon JJ, Swift MD, Bradley M (2010) DNA analysis by dynamic chemistry. *Angew Chem Int Ed Engl* 49:1809–1812.
12. Wang Y, et al. (2009) Direct detection and quantification of abasic sites for in vivo studies of DNA damage and repair. *Nucl Med Biol* 36:975–983.
13. Sutherland BM, Hada M (2006) Spectrum of complex DNA damages depends on the incident radiation. *Radiat Res* 165:223–230.
14. Branton D, et al. (2008) The potential and challenges of nanopore sequencing. *Nat Biotechnol* 26:1146–1153.
15. Deamer DW, Branton D (2002) Characterization of nucleic acids by nanopore analysis. *Acc Chem Res* 35:817–825.
16. Song L, et al. (1996) Structure of staphylococcal α-hemolysin, a heptameric transmembrane pore. *Science* 274:1859–1866.
17. Kasianowicz JJ, Brandin E, Branton D, Deamer DW (1996) Characterization of individual polynucleotide molecules using a membrane channel. *Proc Natl Acad Sci USA* 93:13770–13773.
18. Clarke J, et al. (2009) Continuous base identification for single-molecule nanopore DNA sequencing. *Nat Nanotechnol* 4:265–270.
19. Meller A, Nivon L, Brandin E, Golovchenko J, Branton D (2000) Rapid nanopore discrimination between single polynucleotide molecules. *Proc Natl Acad Sci USA* 97:1079–1084.
20. Wallace EVB, et al. (2010) Identification of epigenetic DNA modifications with a protein nanopore. *Chem Commun* 46:8195–8197.
21. Schibel AEP, et al. (2010) Nanopore detection of 8-oxo-7,8-dihydro-2′-deoxyguanosine in immobilized single-stranded DNA via adduct formation to the DNA damage site. *J Am Chem Soc* 132:17992–17995.
22. Schibel AEP, et al. (2011) Sequence-specific single-molecule analysis of 8-oxo-7,8-dihydroguanine lesions in DNA based on unzipping kinetics of complementary probes in ion channel recordings. *J Am Chem Soc* 133:14778–14784.
23. Vercoutere WA, et al. (2001) Rapid discrimination among individual DNA hairpin molecules at single-nucleotide resolution using an ion channel. *Nat Biotechnol* 19:248–252.
24. Olasagasti F, et al. (2010) Replication of individual DNA molecules under electronic control using a protein nanopore. *Nat Nanotechnol* 5:798–806.
25. Gyarfas B, et al. (2009) Mapping the position of DNA polymerase-bound DNA templates in a nanopore at 5 A resolution. *ACS Nano* 6:1457–1466.
26. Lieberman KR, et al. (2010) Processive replication of single DNA molecules in a nanopore catalyzed by phi29 DNA polymerase. *J Am Chem Soc* 132:17961–17972.
27. Lu S, Li W, Rotem D, Mikhailova E, Bayley H (2010) A primary hydrogen-deuterium isotope effect observed at the single-molecule level. *Nat Chem* 2:921–928.
28. Stoddart D, Heron AJ, Mikhailova E, Maglia G, Bayley H (2009) Single-nucleotide discrimination in immobilized DNA oligonucleotides with a biological nanopore. *Proc Natl Acad Sci USA* 106:7702–7707.
29. Maglia G, Restrepo MR, Mikhailova E, Bayley H (2008) Enhanced translocation of single DNA molecules through a-hemolysin nanopores by manipulation of internal charge. *Proc Natl Acad Sci USA* 105:19720–19725.
30. Rincon-Restrepo M, Mikhailova E, Bayley H, Maglia G (2011) Controlled translocation of individual DNA molecules through protein nanopores with engineered molecular brakes. *Nano Lett* 11:746–750.
31. Banerjee A, et al. (2010) Molecular bases of cyclodextrin adapter interactions with engineered protein nanopores. *Proc Natl Acad Sci USA* 107:8165–8170.
32. Mitchell N, Howorka S (2008) Chemical tags facilitate the sensing of individual DNA strands with nanopores. *Angew Chem Int Ed Engl* 47:5565–5568.
33. Cherf GM, et al. (2012) Automated forward and reverse ratcheting of DNA in a nanopore at 5-Å precesion. *Nat Biotechnol* 30:343–348.
34. Manrao EA, et al. (2012) Reading DNA at single-nucleotide resolution with a mutant MspA nanopore and phi29 DNA polymerase. *Nat Biotechnol* 30:349–353.
35. Kawano R, Schibel AEP, Cauley C, White HS (2009) Controlling the translocation of single-stranded DNA through a-hemolysin ion channels using viscosity. *Langmuir* 25:1233–1237.
36. Japrung D, Henricus M, Li Q, Maglia G, Bayley H (2010) Urea facilitates the translocation of single-stranded DNA and RNA through the a-hemolysin nanopore. *Biophys J* 98:1856–1863.
37. Frelon S, et al. (2000) High-performance liquid chromatography-tandem mass spectrometry measurement of radiation-induced base damage to isolated and cellular DNA. *Chem Res Toxicol* 13:1002–1010.
38. Purnell RF, Mehta KK, Schmidt JJ (2008) Nucleotide identification and orientation discrimination of DNA homopolymers immobilized in a protein nanopore. *Nano Lett* 8:3029–3034.
39. Henrickson SE, Misakian M, Robertson B, Kasianowicz JJ (2000) Driven DNA transport into an asymmetric nanometer-scale pore. *Phys Rev Lett* 85:3057–3060.
40. Muzard J, Martinho M, Mathe J, Bockelmann U, Viasnoff V (2010) DNA translocation and unzipping through a nanopore: Some geometrical effects. *Biophys J* 98:2170–2178.
41. Martinez-Haya B, et al. (2010) Emergence of symmetry and chirality in crown ether complexes with alkali metal cations. *J Phys Chem A* 114:7048–7054.
42. Smetana AJ, Popov AI (1980) Lithium-7 nuclear magnetic resonance and calorimetric study of lithium crown complexes in various solvents. *J Solution Chem* 9:183–196.
43. Izatt RM, Bradshaw JS, Nielsen SA, Lamb JD, Christensen JJ (1985) Thermodynamic and kinetic data for cation-macrocycle interaction. *Chem Rev* 85:271–339.
44. Broido MS, Kearns DR (1982) ^{1}H NMR evidence for a left-handed helical structure of poly(ribocytidylic acid) in neutral solution. *J Am Chem Soc* 104:5207–5216.